Computational issues in using a dual-scale model of the segregation process in a binary alloy

S. Sundarraj
Concurrent Technologies Corporation, Jonestown, Pennsylvania, USA, and
V.R. Voller
Saint Anthony Falls Laboratory, Department of Civil Engineering, University of Minnesota, Minneapolis, Minnesota, USA

Introduction

During the solidification of a metal, on the scale of the process (~meters), three distinct regions can be identified: a solid region, a mushy region and a liquid region. Usually the mushy region consists of a dendritic crystal morphology with a length scale, defined by the secondary arm spacing, on the order or microns (see Figure 1).

Key solidification phenomena occur within the mushy region. Many of these phenomena are associated with both the macro-scale of the process and the micro-scale of the dendrite arm spaces. An important example is segregation of the alloy components. Consider the solidification of a dilute binary alloy with a partition ratio $k_0 < 1$. When the solid forms in the mushy region, the solute phase is rejected into the liquid. At the micro-scale (i.e. the dendrite arm spaces), this solute is redistributed in the solid and liquid phase by diffusion, a process referred to as microsegregation. At the macroscopic scale of the casting, the solute phase is redistributed by fluid flow (driven by thermal and solutal natural convection), a process referred to as macrosegregation. If segregation processes are to be modelled numerically, owing to the complex interaction of the phenomena across a wide range of length scales, innovative computational approaches are required.

In this paper, the computational issues involved in modelling segregation phenomena are examined, with particular emphasis placed on methodologies which can capture the disparate length scales of the problem. Towards this end, a test problem involving the unidirectional solidification, from below, of an aluminum copper alloy is investigated. Modelling this system involves the coupling of a macroscopic model, describing the heat and mass transfer in the

This work was supported by a resource and a travel grant from the Minnesota Supercomputer Institute, University of Minnesota.

International Journal of Numerical Methods for Heat & Fluid Flow
Vol. 7 No. 2/3, 1997, pp. 181-199.

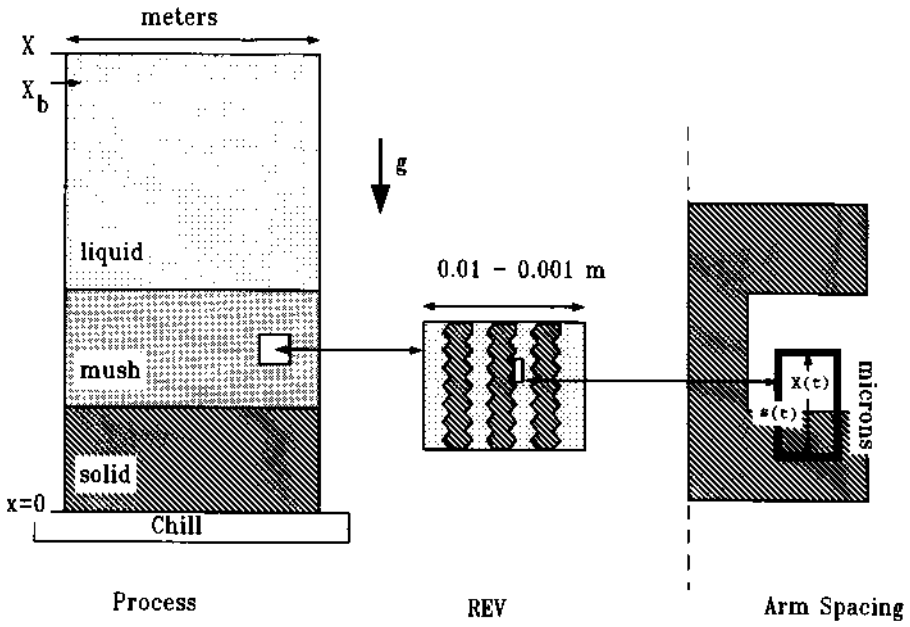

Figure 1.
Length scales in an alloy casting

process as a whole, with a microscopic model that describes the mass transport (microsegregation) in the secondary dendritic arm spaces. This modelling is achieved on introducing a so called “bi-level” grid. A regular macro grid (finite element or finite difference) on the scale of the process is used for the solution of equations describing macroscopic heat and mass transport (the macroscopic model). In the usual manner, values of variables at a macroscopic node are representative of values in a specified control volume surrounding the node. Further, each node point in the macro grid is also associated with a micro grid on which equations describing the microscopic phenomena in the mushy region are solved (the microscopic model). Values obtained with a microscopic model, located at a given macro node point, are taken to be representative of the microscopic behaviour in that node’s control volume. The result of using this bi-level grid is a “dual-scale” segregation model that successfully couples the macro and micro length scales into a single multi-scale treatment. The macroscopic and microscopic models that make up the dual-scale model are established in the literature[1,2] and preliminary findings using the dual-scale model have also been reported[3-5]. The central contribution of the current work focuses on the numerical issues associated with the computational implementation of the dual-scale model.

A test problem

In order to provide a context for the development of a dual-scale segregation model, a problem involving the unidirectional solidification of a dilute aluminum-copper alloy from below is considered. This system has previously

been investigated, both experimentally and numerically, by a number of researchers, e.g.[1,6,7]. A schematic of the process is shown in Figure 1. A liquid aluminum-copper alloy, temperature $T > T_{liq}$ (the liquidus temperature) and nominal solute copper concentration C_o (wt.%), occupies the domain $0 \leq x \leq X$. At time t = 0, the alloy comes into contact with a cold mold, at $x = 0$, convectively cooled such that its temperature is $T < T_{eut}$ (the eutectic temperature). As time proceeds, the alloy will solidify and at any point in time $t > 0$, owing to its multi-component nature, three regions will be identified: a fully solid region; a fully liquid region; and a two-phase (solid and liquid) mushy region with a dendritic crystalline morphology. As solid forms in the mushy region, the copper solute is rejected into the liquid phase ($k_o < 1$ in dilute aluminum-copper alloys) and is subsequently redistributed by mass diffusion at the micro-scale and advection on the scale of the process. It is noted that, since copper is heavier than aluminum, the given system is both thermally and solutally stable and the only fluid flows that give rise to advection are driven by solidification shrinkage as the solid forms. These flows are directed towards the chill face and, as a result, on final solidification a region of +ve segregation $[C] > C_o$ is observed in the vicinity of the chill, see Figure 2; a phenomenon often referred to as inverse segregation. The objective of the dual-scale model

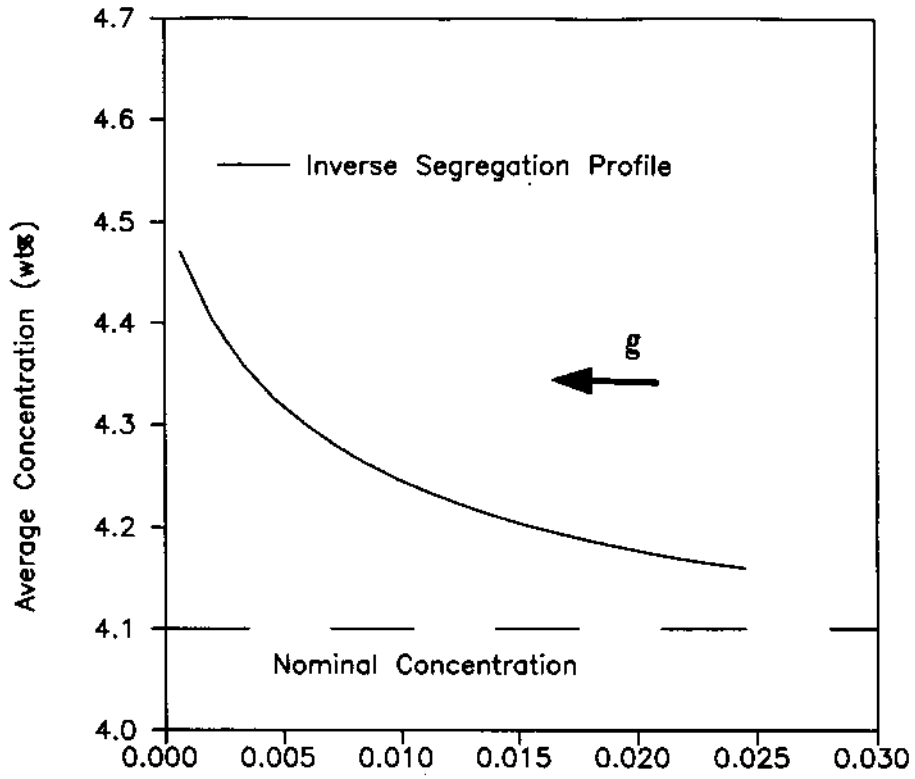

Figure 2. Schematic of the positive inverse segregation profile in the vicinity of the chill

developed in this work will be to predict the level of segregation in the inverse segregation region.

The keys to establishing a dual-scale model that can "capture" both the macro and micro-scale segregation phenomena rest in:

- the definition of suitable macroscopic variables in terms of microscopic variables; and
- the development of a numerical implementation that can bridge across the scales.

Variables

Using a multi-phase volume averaging approach, pioneered in the context of solidification systems by Beckermann and co-workers[8,9], appropriate macroscopic variables are defined on choosing a representative elementary volume (REV) in the mushy region, see Figure 1. The REV is chosen to be larger than the typical microstructure length scale (the secondary arm spaces) but smaller than the characteristic length scale of the process. A typical REV should contain a number of primary dendrite arms and have a size on the order of 0.01-0.001m (i.e. about the size of a typical numerical discretization element[8]). With reference to an aluminum-copper alloy, the following assumptions are made for the REV:

- equilibrium holds at the solid/liquid interface, i.e.

$$C_s^* = k_o C_l^* \tag{1}$$

  where C is the concentration, the subscripts $_1$ and $_s$ refer to the liquid and solid phases respectively and the superscript * denotes values at the solid/liquid interface;
- uniform liquid concentration, C_1, in the liquid phase (the liquid mass diffusion is four orders of magnitude larger than the solid mass diffusion);
- uniform temperature, $T = T_s = T_1$, throughout (the Lewis number for Al-Cu alloys is around 200);
- uniform microstructure, for example see Figure 1a in Ni and Beckermann[8].

These assumptions are reasonably valid for an aluminum-copper system and are consistent with assumptions made in many studies.

On using the above assumptions, it is possible to define mixture variables representative of the REV as a whole:

Mixture density (kg/m$_3$):

$$[\rho] = \int_0^{g_s} \rho_s \, d\alpha + g_l \rho_l \tag{2}$$

Mixture volumetric enthalpy (J/m^3):

$$[\rho H] = c_{p_s} T \int_0^{g_s} \rho_s \, d\alpha + g_l \rho_l c_{p_l} T + g_l \rho_l L \quad (3)$$

Mixture solute density (kg/m^3):

$$[\rho C] = \int_0^{g_s} \rho_s C_s \, d\alpha + g_l \rho_l C_l \quad (4)$$

Mixture concentration (wt.%):

$$[C] = \frac{[\rho C]}{[\rho]} \quad (5)$$

where $0 \leq g_S \leq 1$ is the solid fraction of the REV. The variables C and ρ define microscopic point quantities of concentration and density in the REV. In order to evaluate the integrals in the above expressions, the distribution of the solute in the solid is required; a distribution that is controlled by the microsegregation process. Hence the definition of the macroscopic variables requires the modelling of the micro-scale processes; a situation that motivates the development of a dual-scale model.

The bi-level grid

In general, the role of a numerical discretization is to cover the domain of interest with a grid of node points and assign variable values to the node points. These values are then taken as representative of the variable values over a finite volume that surrounds the node point. In the case of the dual-scale modelling of segregation, the numerical discretization needs to be able to capture both the macro scale (heat and mass transfer at the process scale) and micro-scales (mass diffusion in the secondary arm spacings). This is achieved on introducing a bi-level grid. In the first place the macroscopic scale of the process is covered by a grid of node-centred control volumes (see Figure 3). As noted above, a typical volume size in this macro grid will be on the order of the REV. Macro nodal grid values, viz. temperature T, mixture density[ρ] , mixture enthalpy[ρH] and mixture solute density[ρC] are representative values for the surrounding control volume. Further, it is assumed that the microscopic state at the node point is representative of the microscopic state in the surrounding control volume. The microscopic state of the macro node is determined on solving for the solid mass diffusion in the REV. This solution is carried out on a micro-scale grid, centred on the macro node, nominally associated with a secondary arm spacing in the REV (see Figure 3). The contention is that solution of the micro-scale phenomena (segregation and arm coarsening) on this micro grid, under the constraints of the macro nodal values, will be representative of the micro-scale condition in the macro control volume (REV) as a whole. This contention is partially supported on noting that previous predictions obtained with the micro-scale model[2] to be used in this work are in close agreement with

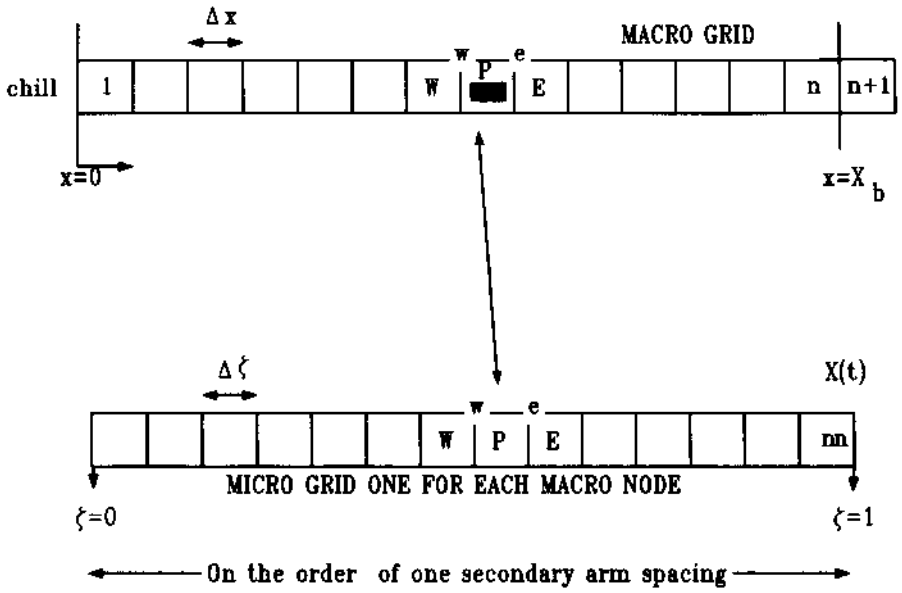

Figure 3.
The bi-level grid used in the dual scale model

experimental measurements (see Table 6 in[2]). Since, by their nature, micro-scale experimental measurements are volume averaged over an REV, it can be concluded that the micro-scale model is indeed representative of the surrounding REV.

The dual-scale model

Overview

In operation, at each point in time, the dual-scale model involves two major steps:

(1) The modelling of the process scale with prediction of the macroscopic variables. This modelling is carried out on the macro grid in Figure 3 and employs an explicit time integration.

(2) The modelling of the micro phenomena. This modelling is carried out on the micro grids in Figure 3, one micro grid associated with each macro node. The time stepping is implicit and the calculations are constrained by the macro-scale predictions from step 1.

The operation of the macro and micro-scale models are described in detail below.

Macro-scale assumptions

On the scale of the process the key assumptions for the model are:

- The domain is one-dimensional and occupies the space $0 \leq x \leq X_b$; where, following Voller and Sundarraj[1], the Value $X_b < X$ represents the extent

of the macroporosity-free region, i.e. throughout the process it can be assumed that there is always enough liquid in the region $x > X_b$ to feed the shrinkage.

- There is no mass flow across the line $x = 0$, i.e. no surface exudation.
- The specific heats, c_s and c_1, and thermal conductivities, K_s and K_1, are constant within each phase.
- The latent heat of fusion L is constant.
- The solidus and liquidus lines in the phase diagram, Figure 4, are non-linear functions of temperature, i.e.

$$C_s^* = F_s(T); \qquad C_l^* = F_l(T) \tag{6}$$

- Using expressions derived by Ganesan and Poirier[10], the solid and liquid densities, ρ_s and ρ_l, are functions of the liquid solute

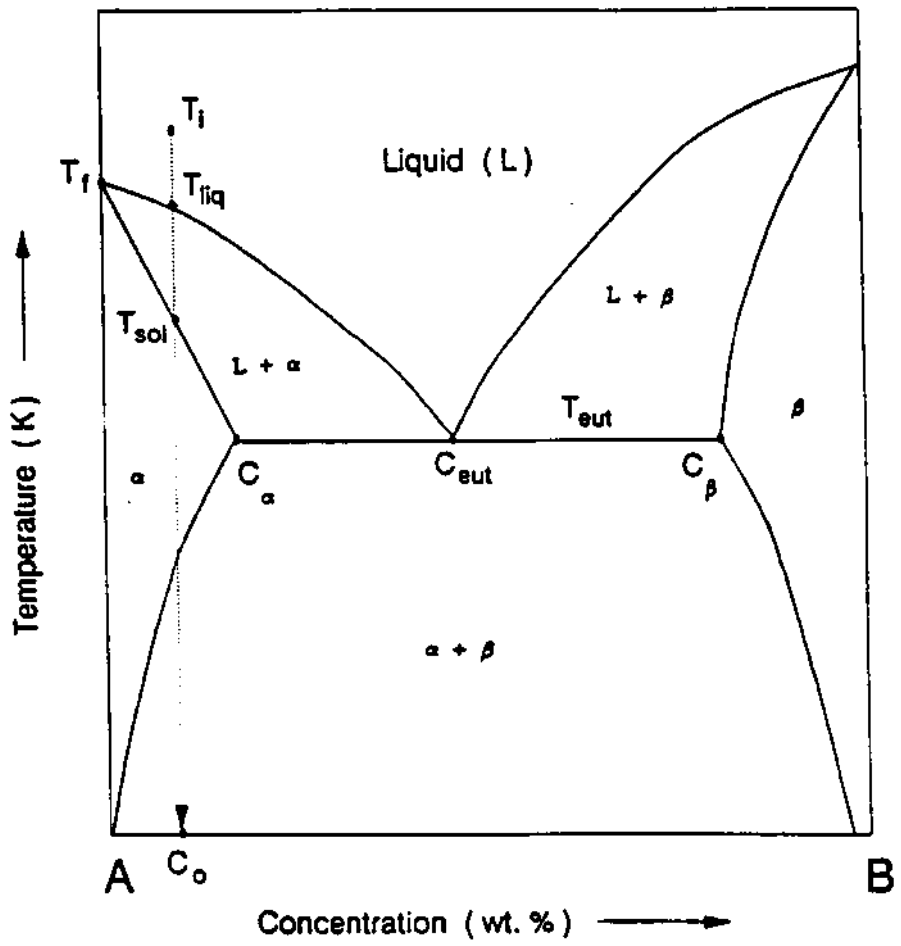

Figure 4.
A section of the phase diagram for aluminum-copper alloys

concentration, C_1. It is important to note that the solid density relationship depends on the level of local (microscopic) mass diffusion in the solid; in this work for low and moderate mass diffusion the density ρ_s^1 in Table I will be used, whereas for large mass diffusion the density ρ_s^2 in Table I will be used.

- The solid is stationary, essentially a columnar dendritic structure or a consolidated equiaxed structure.
- The liquid velocity u_1 is uniform over the REV (i.e., dispersion terms are neglected).
- The formation of micro porosity in the region $0 \leq x \leq X_b$ is neglected.

Appropriate thermal data for the aluminum-copper alloy are given in Table I. Note that the choice of convective cooling at the mold, h_b, is made in order to match the experimental conditions used by Kato and Cahoon[7].

Macro-scale governing equations

With the above assumptions, single domain equations describing the inverse segregation process in the domain of the test problem $0 < x < X_b$ can be derived

Property	Value	Unit
C_{p_s}	900	J/kg-K
C_{p_1}	1,100	J/kg-K
h_{amb}	$1{,}684.21 - 4.3443\ t + 0.00449561\ t^2$	W/m^2-K
K_1	100	W/m-K
K_s	200	W/m-K
L	3.95×10^5	J/kg
T_{amb}	293	K
T_i	1,020	K
X_b	0.1323	m
ρ_1[10]	$2{,}358.5 + 21.685\ C_1 + 7.2914 \times 10^{-2}\ C_1^2 - 7.2351 \times 10^{-4}\ C_1^3$	kg/m^3
ρ_s^1[10]	$2{,}564.7 + 1.4023\ C_1$	kg/m^3
ρ_s^2[10]	$2{,}558.1 + 2.1743\ C_1 + 0.060433\ C_1^2$	kg/m^3
ρ_s^{eut}	3,409	kg/m^3
C_{eut}	33.2	wt%
C_o	4.1	wt%
C_1(T)	$3{,}371.84 - 11.4464\ T + 0.01333\ T^2 - 5.2955 \times 10^{-6}\ T^3$	wt%
C_s(T)	$47.1311 - 0.0505141\ T$	wt%
D_1	$1.05 \times 10^{-7} \exp(-2{,}856/T)$	m^2/s
D_s	$0.29 \times 10^{-4} \exp(-15{,}610/T)$	m^2/s
k_o(T)	$C_s(T)/C_1(T)$	
T_{eut}	821.2	K
T_f	933.2	K
T_{liq}	921.73	K
ΔH_f	1.07×10^9	J/m^3
γ	0.093	J/m^3

Table I.
Thermal properties of A1-Cu alloy system

on combing the two-phase volume-averaged equations presented by Ni and Beckermann[8]. These macroscopic governing equations are[1]:

Heat transfer:

$$C^{APP}\frac{\partial T}{\partial t} + \frac{\partial}{\partial x}(\rho_l u c_l T) + \frac{\partial}{\partial x}(\rho_l u L) = \frac{\partial}{\partial x}\left([K]\frac{\partial T}{\partial x}\right) \tag{7}$$

Solute transfer:

$$\frac{\partial[\rho C]}{\partial t} + \frac{\partial}{\partial x}(\rho_l u C_l) = 0 \tag{8}$$

and mass continuity:

$$\frac{\partial[\rho]}{\partial t} + \frac{\partial}{\partial x}(\rho_l u) = 0 \tag{9}$$

where

$$[K] = g_s K_s + g_l K_l \tag{10}$$

is a mixture thermal conductivity

$$u = g_l u_l \tag{11}$$

is the "system velocity" and

$$C^{APP} = \frac{d[\rho H]}{dT} \tag{12}$$

is an apparent specific heat. Appropriate boundary conditions for the above macroscopic equations are: at $x = 0$:

$$F = 0; \qquad [K]\frac{\partial T}{\partial x} = h_{amb}(T_{amb} - T|_{x=0}); \qquad \frac{\partial C_l}{\partial x} = 0 \tag{13}$$

where h_{amb} is the heat transfer coefficient, T_{amb} is the ambient temperature of the chill and $F = \rho_l u$ is the mass flow rate of liquid per unit area.

At $x = X_b$,

$$F = F_b = \rho_l u_b; \qquad \frac{\partial T}{\partial x} = 0; \qquad \frac{\partial C_l}{\partial x} = 0 \tag{14}$$

where F_b is the mass flow rate of the liquid metal per unit area that enters the system to compensate for the shrinkage in $0 < x < X_b$. Note that this mass flux will result in a convective heat flux and solutal mass flux at $x = X_b$ of the form

$$q_h = F_b (c_l T|_{x=X_b} + L) \tag{15}$$

and

$$q_c = F_b C_l|_{x=X_b} \tag{16}$$

Macro-scale discretization details

An explicit time integration of the above equations based on a node-centred uniform grid of n control volumes[11] leads to the following set of discrete equations:

Heat transfer:

$$C_P^{APP} T_P = a_W T_W^{\circ} + a_E T_E^{\circ} - a_P T_P^{\circ} + S \tag{17}$$

where

$$a_W = [K]_w \frac{\Delta t}{(\Delta x)^2} \; ; \; a_E = [K]_e \frac{\Delta t}{(\Delta x)^2} \; ; \; a_P = a_W + a_E + C^{APP}$$

$$S = \frac{\Delta t}{\Delta x} \left(c_l \left(F_w^{\circ} T_P^{\circ} - F_e^{\circ} T_E^{\circ} \right) + \left(F_w^{\circ} - F_e^{\circ} \right) L \right) \tag{18}$$

Solute transfer:

$$[\rho C] = [\rho C]_P^{\circ} + \frac{\Delta t}{\Delta x} \left(F_w^{\circ} C_{l_P}^{\circ} - F_e^{\circ} C_{l_E}^{\circ} \right) \tag{19}$$

Mass continuity:

$$F_e = F_w + \frac{\Delta x}{\Delta t} \left([\rho]_P^{\circ} - [\rho]_P \right) \tag{20}$$

where the convective terms have been “upwinded” assuming that the flow is towards the chill face. In the above equations,

$$[K]_e = \left(\frac{[K]_P + [K]_E}{2} \right) ; \text{ etc.} \tag{21}$$

$$F = \rho_l u \tag{22}$$

is the mass flow rate of liquid per unit area, the superscript $^{\circ}$ represents old values, the subscripts *w* and *e* represent the west and east faces of control volume *P*, and the subscripts *W* and *E* denote the nodes to the west and east of node P (see Figure 3). Further, values for the nodal temperature T_{n+1} and nodal liquid concentration $(C_1)_{n+1}$ are evaluated via linear extrapolation. The apparent heat capacity C^{APP}, at a given node, is approximated in the following manner:

$$C^{APP} = \begin{cases} \rho_l^i c_l, & T^{\circ} > T_{liq} \\ \dfrac{[\rho H]^{\circ} - [\rho H]^{oo}}{T^{\circ} - T^{oo}}, & T_{liq} \geq T^{\circ} \geq T_{eut} \\ \rho_s c_s, & T^{\circ} < T_{eut} \end{cases} \tag{23}$$

where superscript ^{oo} refers to the values calculated two time steps behind the current time step.

The solution approach

The numerical solution of the above equations consists of three basic steps:

(1) With the $[\rho H]$, T, C_1 and F field values at the previous time step, the current time step values of temperature T and mixture solute density $[\rho C]$ are determined explicitly from equations (17) and (19).

(2) A micro-scale treatment, carried out on the micro grids in Figure 3, which determines the microsegregation in the solid phase of the REV, is invoked. This treatment provides current time-step values for $[\rho]$,$[\rho H]$ and C_1.

(3) Finally, the current and previous values of the density fields, are used, in equation (20), to determine the flow field to be used in the next time step.

Clearly a key step in the above algorithm is the micro-scale treatment. In previous numerical models of segregation, the common approach is to arrive at a micro-scale treatment on making limiting assumption about the nature of the solute diffusion in the solid phase of the REV. The extreme cases of the lever assumption, complete mass diffusion in the REV solid phase,and the Scheil assumption, no mass diffusion in the REV solid, are often invoked as micro-scale models. In the current study, however, a more precise treatment of micro-scale segregation phenomena, involving finite solid mass diffusion and microstructural evolution in the REV, will be used.

Micro-scale assumptions

The micro-scale treatment is based on a previously presented model of microsegregation[2] in a dendritic binary alloy. Additional assumptions to those already presented are:

- The microsegregation domain is one-dimensional and nominally associated with a secondary dendrite arm spacing (see Figure 1).
- Owing to the coarsening process, the size of the microsegregation domain $X(t)$ increases with time (the model proposed by Roosz *et al.*[12] will be used in this work).
- The moving solid/liquid interface, $s(t)$, is planar and sharp.
- Mass transfer in the domain is controlled by diffusion alone.
- Primary and eutectic undercoolings are neglected.

The micro-scale equations

The microsegregation problem requires the separate solutions of a solid and liquid mass diffusion equation in an expanding domain, $0 < x < X(t)$. On defining a variable V, the "chemical activity"

$$V = \begin{cases} C_s & x \le s(t) \\ k_o(T)\, C_l & x > s(t) \end{cases} \tag{24}$$

and using the Landau transformation

$$\xi = \frac{x}{X(t)} \tag{25}$$

the problem can be reduced to a single equation in a fixed domain $0 \le \xi \ge 1$, viz.,

$$\frac{\partial(\rho C)}{\partial t}\Big|_{\xi} = \frac{1}{X^2}\frac{\partial}{\partial \xi}\left[\rho D \frac{\partial V}{\partial \xi}\right] + \frac{1}{X}\frac{dX}{dt}\left[\frac{\partial(\xi \rho C)}{\partial \xi} - \rho C\right] \tag{26}$$

where

$$\rho D = \left[\rho_s (1-g_1^L) D_s + \rho_1 g_1^L \left(\frac{D_1}{k_o}\right)\right] \tag{27}$$

$$\rho C = \left[\rho_s (1-g_1^L) + \rho_1 g_1^L \left(\frac{1}{k_o}\right)\right] V \tag{28}$$

$$\rho = \rho_s (1-g_1^L) + \rho_1 g_1^L \tag{29}$$

D is the mass diffusion coefficient[m^2/s] and g_1^L is the local liquid fraction at a point in the micro domain. The boundary conditions for equation (26) are

$$\frac{\partial V}{\partial \xi} = 0 ; \qquad \text{at } \xi=0 \text{ and } \xi=1 \tag{30}$$

and

$$q_C = \frac{d}{dt}([\rho C] X) ; \quad \text{at } \xi=1 \tag{31}$$

The application of this last boundary condition requires the specification of a mixture solute density history [ρC] and a coarsening history $X(t)$; in addition, calculation of other model parameters requires a cooling history for the domain $T(t)$. A successful model for the coarsening is that of Roosz *et al.*[12],

$$X(t)^3 = 13.125 \int_0^t M_c \, dt \tag{32}$$

The coarsening parameter M_c is given by

$$M_c = \left[\frac{\gamma D_1 T}{m_1 (1-k_o(T)) \Delta H_f C_1}\right] \tag{33}$$

where γ is the interfacial surface energy, ΔH_f is the volumetric latent heat of fusion and $m_1 = (T_f - T_{eut})/C_{eut}$ is the representative liquidus slope (T_f is the fusion temperature and C_{eut} is the eutectic concentration of the alloy); appropriate data and units are given in Table I. In a general application of the above microsegregation model, the mixture solute density[ρC](t) and cooling $T(t)$ histories are externally provided. In the current application, however, these values will be provided by the explicit solution of the macro equations, equations (17) and (19) above.

Micro-scale solution

On a micro grid in Figure 3, consisting of nn equally-spaced control volumes of size $\Delta\xi$, a fully time implicit central difference discretization of equation (26) leads to the non-linear discrete equation

$$a_p V_p = \rho_p^o E_p^{old} V_p^o + \rho_w \Gamma_w^C V_w + \rho_e \Gamma_e^C V_E + S \tag{34}$$

with the coefficients defined as

$$a_P = \rho_P E_P + \rho_w \Gamma_w + \rho_e \Gamma_e \tag{35}$$

$$\Gamma_e = \left(\frac{D_E + D_P}{2}\right) \frac{\Delta t}{X^2 (\Delta \xi)^2} \quad ; \quad \text{etc.,} \tag{36}$$

$$\rho_e = \left(\frac{\rho_E + \rho_P}{2}\right) ; \text{ etc.,} \tag{37}$$

$$E_P = (1 - g_P^L) + \left(\frac{g_P^L}{k_o}\right) ; \text{ etc.,} \tag{38}$$

Using a central difference replacement

$$S = \frac{\Delta t}{X} \frac{dX}{dt} \left[\left(\frac{(\xi \rho C)_e - (\xi \rho C)_w}{\Delta \xi} \right) - \rho_P E_P V_P \right] \tag{39}$$

where

$$\begin{aligned} (\xi \rho C)_e &= \left(\frac{\xi_E \rho_E E_E V_E + \xi_P \rho_P E_P V_P}{2} \right) \\ (\xi \rho C)_w &= \left(\frac{\xi_P \rho_P E_P V_P + \xi_W \rho_W E_W V_W}{2} \right) \end{aligned} \tag{40}$$

At the node adjacent to the boundary $\xi = 0$

$$\Gamma_w^c = 0 , \quad (\xi \rho C)_w = 0 \tag{41}$$

and at the node adjacent to the boundary $\xi = 1$

$$\Gamma_e^c = 0, \quad (\xi \rho C)_e = q_c \left(\frac{dX}{dt}\right)^{-1} \tag{42}$$

In solving equation (34), at a given time step Δt, the following points are noted:

- Domain values of temperature T and mixture solid density $[\rho C]$ are known, calculated by the explicit step in the macro model.
- There will be only one cell in the domain in which $0 < g_P^L < 1$. All the other cells will be solid $g_P^L = 0$ or liquid $g_P^L = 1$.
- On convergence, the nodal $\underline{V}$ field will be such that, if the phase front is located in control volume P, the nodal value V_P will satisfy the equilibrium condition

$$V_P = F_E^{-1}(T) \tag{43}$$

An iterative solution is employed. The seven key steps are:

(1) From the known domain temperature (the nodal temperature at the associated macro node point), the current equilibrium concentration value V_{equ} is calculated using the phase diagram relationship

$$V_{equ} = F_E^{-1}(T) \tag{44}$$

(2) The temperature- and concentration-dependent properties, e.g. coarsening $X(t)$, are then evaluated.

(3) At iteration m, the coefficients in equation (34) are set up according to the most current liquid fraction field. At the phase change node, the unique node where $0 < (g_P^L)^m < 1$, the coefficient a_P is set to a large value (e.g. BIG = 10^{25}) and the source term to S = BIG V_{equ}, thereby forcing the node to take the required equilibrium value.

(4) With these coefficients, equation(34) is solved to determine the concentration field, V.

(5) The local nodal liquid fraction field, g_1 is then updated.

(6) Steps 3-5 are repeated until the concentration field, V, and liquid fraction field g_1 are consistent.

(7) The values required for the next explicit step on the macro grid are then calculated as

$$C_1 = \Delta\xi \left[\frac{\rho_1 (g_P^L) V_{equ}}{k_o} + \sum_{I=P+1}^{nn} \rho_I \frac{V_I}{k_o} \right] \tag{45}$$

$$[\rho] = \Delta\xi \left[\sum_{I=1}^{P-1} \rho_I + \left[\rho_s (1-(g_P^L)) + \rho_1 (g_P^L) \right] + \sum_{I=P+1}^{nn} \rho_I \right] \tag{46}$$

$$[\rho H] = \Delta\xi \left[\sum_{I=1}^{P-1} \rho_I c_s T + \left[\rho_s c_s T (1-(g_P^L)) + \rho_1 c_1 T (g_P^L) \right] + \sum_{I=P+1}^{nn} \rho_I c_1 T \right] \tag{47}$$

where the nodal densities are calculated by the expressions in Table I on setting nodal values of the liquid concentration $C_{1I} = V_I/k_o$.

The major component in the solution algorithm is updating the nodal liquid fraction field, i.e. step 5. This is achieved on selecting the nodal liquid fraction field to ensure overall mass balance in the domain. If P is the phase change node, then the overall mass balance is given by

$$[\rho C](t) = \Delta\xi \left[\sum_{I=1}^{P-1} \rho_I V_I + \left[\rho_1 (1-(g_P^L)^{m+1}) + \frac{\rho_s (g_P^L)^{m+1}}{k_o} \right] V_{equ} + \sum_{I=P+1}^{nn} \rho_I \frac{V_I}{k_o} \right] \tag{48}$$

where the superscript $^{m+1}$ denotes the most current iterative value of g_P^L and the value of $[\rho C]$ is obtained from the macro-scale calculation. On rearrangement, equation (48) can be used to obtain the value of g_P^L at node P. In practice, equation(48) is applied at every node with the correction

$$\begin{aligned} &\text{if } g_P^L > 1 \text{ then } g_P^L = 1 \\ &\text{if } g_P^L < 0 \text{ then } g_P^L = 0 \end{aligned} \tag{49}$$

to account for the non-phase change nodes and nodes which have undergone phase change in the time step.

The dual-scale implementation

In summary, at a given time step, the four-step operation of the dual-scale model is as follows:

(1) Current time-step values of the nodal $\underline{T}$ and $[\rho\underline{C}]$ fields are obtained on the explicit solution of equations (17) and (19).

(2) If, at any give node, the predicted temperature is in the range

$$T_{eut} < T_I < T_{liq} \tag{50}$$

the micro model outlined above is implemented and values of $[\rho]$, $[\rho H]$ and C_1, required for the next time step, are calculated. Convergence of the microscopic model takes between three and four iterations per call.

(3) If the macroscopic nodal temperature, predicted by equation (17), falls below the eutectic temperature, T_{eut}, the micro model is not called and a standard explicit enthalpy treatment, which fixes $T_p = T_{eut}$ until solidification is complete, is employed to determine $[\rho H]$ directly from equation (17).

(4) The calculation of the current flow field F terminates the calculations in the time step.

The dual-scale model is used to determine the inverse segregation region in the unidirectional solidification of the Al-4.1%Cu alloy shown in Figure 1; appropriate data are given in Table I.

In the numerical implementation, a grid of 100 equally-spaced macro node points is used. Each macro node point is associated with a micro grid of 100 equally-spaced nodes. A common time step of $\Delta t = 0.0085$ seconds is employed, a value that is restricted by the need to satisfy the stability requirement of the macro model. Simulations are carried out until the first 20 nodes in the macro domain have completed solidification (about three minutes of real time). The computational requirement amounts to about 15 minutes of CPU on a Silicon Graphics R4000 workstation.

Results

Validation

The mechanism of coupling between the micro and macro components in the dual-scale model is validated by comparing the current model predictions with the previous inverse segregation model presented by Voller and Sundarraj[1]; a model which uses the extreme assumption of no solid state mass diffusion in the REV solid (a Scheil assumption). For this comparison, in the dual-scale model, a constant partition coefficient $k_o = 0.172$ is used, a constant arm spacing of $X_{fixed} = 23$ microns is assumed (i.e. no-coarsening) and the Scheil assumption is modelled by setting $D_s = 10^{-20}$. Under these conditions, the dual-scale model predictions of the concentration profile $[C](x)$, in the chill face region, are in very close agreement with the results obtained with the single-scale macro model

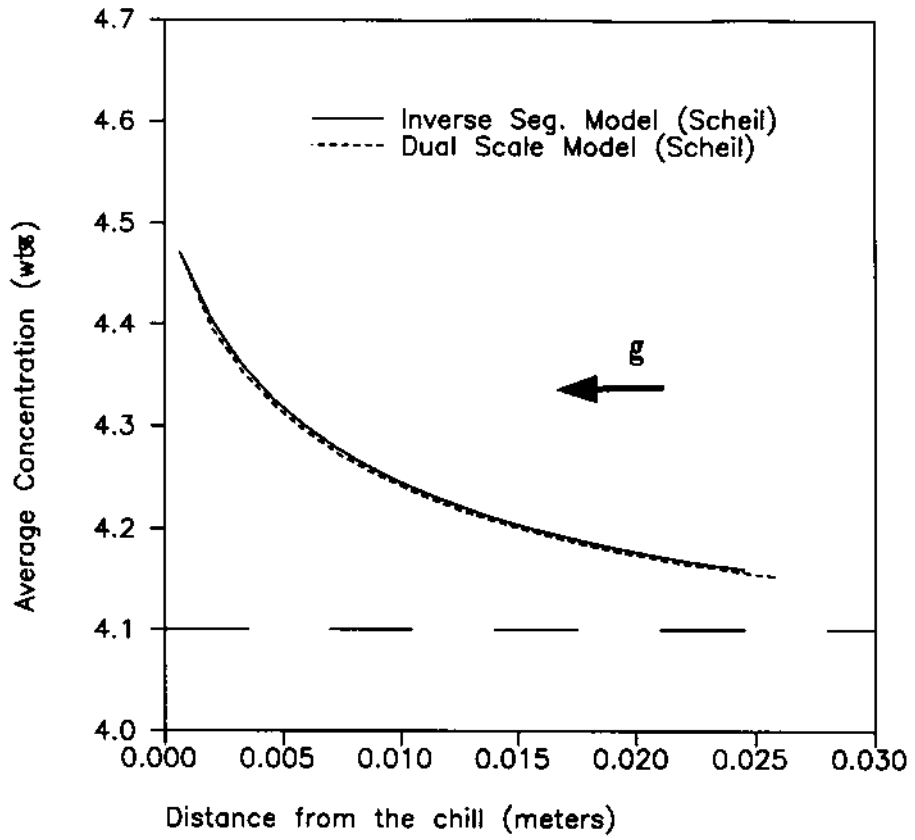

Figure 5.
Validation of the dual scale model

used by Voller and Sundarraj[1] (see Figure 5); results that are in reasonable agreement with experiments, see Figure 10 in reference[1].

Micro-scale effects

Previous inverse segregation models[1,6,7] are single-scale models that use limiting assumptions for dealing with the micro scale. Voller and Sundarraj[1] assume, at the micro scale, zero mass diffusion in the solid and a fixed microstructure. Diao and Tsai[6] also assume a fixed microstructure but make the opposing assumption of complete diffusion in the REV solid (the lever assumption). The major contribution of the dual-scale model outlined above is that it allows for a more exact treatment of the micro scale; in particular the effects of coarsening (non-constant microstructure) and finite solid state diffusion (back diffusion) can be considered. Figure 6 shows the effects, on the inverse segregation profile, of including a more comprehensive treatment of the micro-scale effects. The solid line, in Figure 6, is the base-line comparison, obtained on assuming constant microstructure and zero (very small) back diffusion; the large dashed line is the segregation profile obtained when

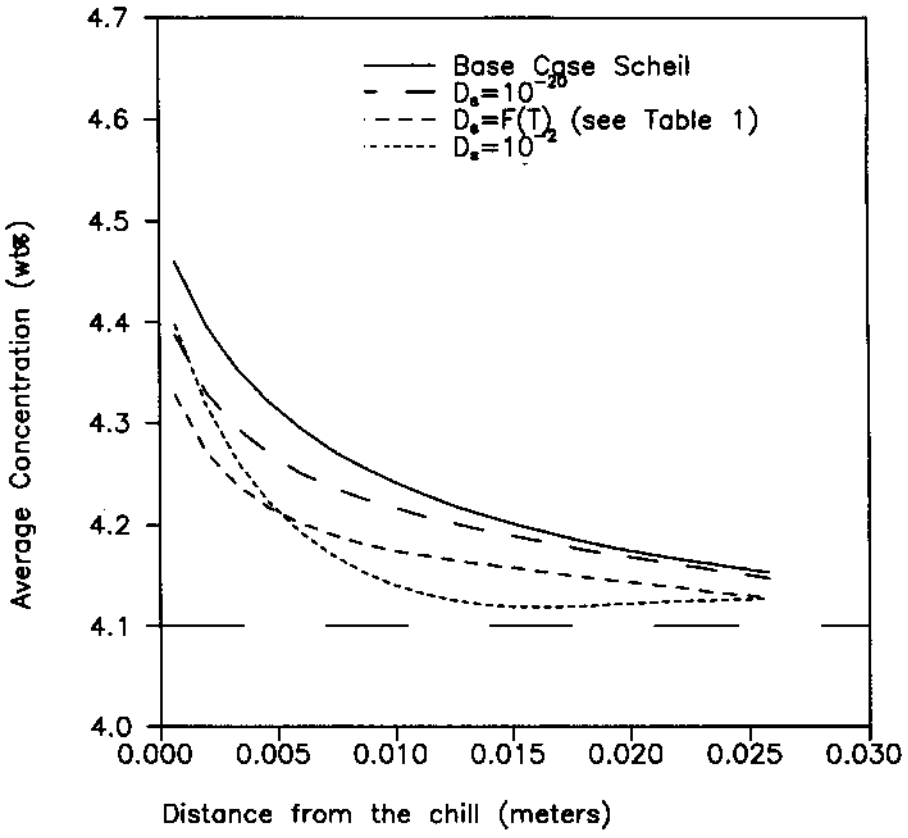

Figure 6.
Effect of the micro scale on macro inverse segregation

coarsening is included; the intermediate dashed line is the segregation profile predicted when the full dual-scale model is implemented using the data in Table I; the small dashed line is the prediction when a larger back diffusion (approaching a lever assumption) is included in the micro component of the dual-scale model. On reference to the results in Figure 6, the effects of including a micro-scale treatment are clearly evident. The driving mechanism in these results is the amount of eutectic formed. The difference between the solid and liquid eutectic densities is significant and, as a result, the more eutectic formed, the greater the solidification shrinkage and the greater the flow back of solute-enriched material towards the chill at $x = 0$. In the dual-scale model, the introduction of both back diffusion and coarsening tends to reduce the amount of eutectic formed at the micro scale[2], with the net result that the level of macrosegregation in the chill-face region is reduced. The results in Figure 6 also show the impact of the choice of density model on the inverse segregation predictions. From the above arguments, one would expect that the level of segregation with a large solid mass diffusion would under-predict all the others; in fact, in the near chill region, the opposite behaviour is observed (see the short

dashed curve in Figure 6). This is because, when a large (approaching complete) diffusion is assumed, the appropriate density model for the solid phase, ρ_s^2 in Table I leads to a larger solidification shrinkage in the early part of the solidification and, as a result, an enhanced level of inverse segregation.

Conclusions

Segregation during the solidification of an alloy is a process that occurs across a wide range of length scales. The central objective of this paper has been to introduce the numerical mechanics required to build a comprehensive model which can realistically account for the key macro- and micro-scale segregation processes during the solidification of a binary alloy. The result has been the introduction of a so called "dual-scale" model. The principal numerical feature in this model is the use of a bi-level grid, in which each node point in the macro-scale grid is associated with a micro-scale grid. A macro-scale transport model, involving heat transfer and convection of solute, is implemented on the macro grid. On each micro grid a micro-scale model, accounting for mass diffusion and microstructure evolution, is implemented. In using this bi-level grid in the dual-scale model, the underlying assumption is that results obtained on the micro grid are representative of the micro-scale phenomena in the control volume surrounding the associated macro control volume. This assumption, through the volume-averaged definition of macro-scale variables, allows for the natural coupling between the macro and micro scales.

The components of the dual-scale model are based on stand-alone single-scale macrosegregation and microsegregation models that have been previously developed and validated[1,2]. In this paper, the operation of the dual-scale model has been validated on comparing its performance with a single-scale macrosegregation model under the limiting assumptions of fixed microstructure and zero solid diffusion. Further, the effectiveness of the dual-scale model has been demonstrated on investigating the effects of micro-scale phenomena on the prediction of inverse macrosegregation during the unidirectional casting of a binary Al-Cu alloy. The predictions indicate that a more exact accounting of the micro scale can effect the macro-scale predictions.

As noted in the introduction, the aim of this paper has been to outline the basic numerical operation of the dual-scale model. With the model in place, there are a number of interesting and worthwhile studies related to the metallurgy that can be carried out. Preliminary studies can be found in the thesis by Sundarraj[3] and recent papers by Sundarraj and Voller[4,5].

References

1. Voller, V.R. and Sundarraj, S., "A model of inverse segregation: the role of microporosity", *International Journal of Heat and Mass Transfer*, Vol. 38, 1995, pp. 1009-18.
2. Voller, V.R. and Sundarraj, S., "Modelling of microsegregation", *Mat. Sci. and Tech.*, Vol. 9, 1993, pp. 474-81.
3. Sundarraj, S., "A dual length scale model of segregation phenomena during binary alloy solidification", PhD thesis, University of Minnesota, MN, 1994.

4. Sundarraj, S. and Voller, V.R., "Effects of microscale phenomena and density in modelling macrosegregation", in Cross, M. *et al.* (Eds), *Modelling of Casting, Welding and Advanced Solidification Processes VI*, TMS, Warrendale, PA, 1995.
5. Sundarraj, S. and Voller, V.R., "A dual-scale model of segregation phenomena", in Beckermann, C. *et al.* (Eds), *Transport Phenomena in Solidification*, HTD-Vol. 284, ASME, New York, NY, 1994.
6. Diao, Q.Z. and Tsai, H.L., "Modeling of solute redistribution in the mushy zone during solidification of aluminum-copper alloys", *Metall. Trans. A*, Vol. 24, 1993, pp. 963-73.
7. Kato, H. and Cahoon, J.R., "Inverse segregation in directionally solidified Al-Cu-Ti alloys with equiaxed grains", *Metall. Trans. A*, Vol. 16, 1985, pp. 579-87.
8. Ni, J. and Beckermann, C., "A volume averaged two-phase model for transport phenomena during solidification", *Metall. Trans. B*, Vol. 22, 1991, pp. 349-61.
9. Wang, C.Y. and Beckermann, C., "A multiphase solute diffusion model for dendritic alloy solidification", *Metall. Trans. A*, Vol. 24, 1993, pp. 2787-802.
10. Ganesan, S. and Poirier, D.R., "Densities of aluminum-rich aluminum-copper alloys during solidification", *Metall. Trans. A*, Vol. 18, 1987, pp. 721-3.
11. Patankar, S.V., *Numerical Heat Transfer and Fluid Flow*, Hemisphere, Washington, DC, 1980.
12. Roosz, A., Halder, E. and Exner, H.E., "Numerical calculation of microsegregation in coarsened dendritic microstructure", *Mat. Sci. and Tech.*, Vol. 2, 1986, pp. 1149-55.